JAST, Vol. 7, No. 2, pp 107–122

JAST
Journal of Aerospace Science and Technology

Solution of Thermo-Fluid Problems in Bounded Domains via the Numerical Panel Method

A. Ashrafizadeh[1], **A. A. Hosseinjani**[2]

The classical panel method has been extensively used in external aerodynamics to calculate ideal flow fields around moving vehicles or stationary structures in unbounded domains. However, the panel method, as a somewhat simpler implementation of the boundary element method, has rarely been employed to solve problems in closed complex domains. This paper aims at filling this gap and discusses the numerical solution of the Laplace equation in bounded domains via the numerical panel method. It is shown that the panel method is an efficient and accurate computational algorithm for the solution of this class of problems. Several test cases in heat conduction and internal ideal flow are presented to show that the numerical panel method can be used in closed domains regardless of the complexities in the geometry and/or boundary conditions.

NOMENCLATURE

$\vec{V}_\infty$	Free stream velocity
n	Normal vector on the body
x, z	Coordinates of an arbitrary point
$q_{B,j}$	Flux influence coefficient in NPM equations
$T_{I,j}$	Temperature influence coefficient in NPM equations
c	A constant parameter in Robin boundary condition
q	Heat flux
T	Temperature
h_C	Convection heat transfer coefficient ($h_C = 40W/m^2.K$)
k_C	Conduction heat transfer coefficient ($k_C = 177W/m.K$)
e_T	Percentage of temperature error
$e_T^{\max}$	Maximum percentage of temperature error
K, K', K''	Constant parameters
$\tilde{T}$	Temperature calculated by NPM
$O(\cdots)$	The order of magnitude
h	Length of the panel
$\partial\tilde{T}/\partial n$	Temperature gradient calculated by NPM
$\vec{V}_A$	Velocity vector at a nearby point A
r	Distance between panel and an arbitrary point. Figure 1c
e_q	Percentage of heat flux error
$I_{i,j}$	Location of an arbitrary point in the domain. Figure 2d
N	Total number of panels
x_C, z_C	Coordinates of the center of a panel
B	Location of an arbitrary point on the boundary of domain. Figure 2d
a_P	The influence of the singularity panel P on its corresponding collocation point
a_{nb}	The influence of the singularity panel nb on the collocation point P
C_p	Pressure coefficient

Greek Symbols

Ω	The solution domain
σ	Source (sink) strength

1. *Associate Professor, Corresponding Author, Dept. of Mech. Eng., K.N. Toosi Univ. of Tech., Tehran, Iran, Email: ashrafizadeh@kntu.ac.ir.*
2. *M.Sc. Student, Dept. of Mech. Eng., K.N. Toosi Univ. of Tech., Tehran, Iran.*

μ	Doublet strength
Γ_b	The boundary of the solution domain
δ	Distance between a panel and it's collocation point
δx_i	Distance between a panel and it's collocation point (x-component)
δy_i	Distance between panel and it's collocation point (y-component)
α	The angle between the x axis and the panel direction, Shown in Figure 1c
$\bar{\Gamma}_b$	The boundary Γ_b approximated by the panels

INTRODUCTION

In the classical field numerical solution techniques, such as Finite Difference Method (FDM), Finite Element Method (FEM) and Finite Volume Method (FVM), the boundary Γ_b and the solution field Ω are both discretized to numerically impose the boundary conditions and to approximately satisfy the governing equations at the internal grid points as well [1,2]. It has been known for a long time that the solution field in a class of problems governed by elliptic differential operators can be constructed by computational procedures which only carry out the integration of a simplified form of the governing equations along the boundary of the domain. In general, the Boundary Integral Methods (BIM) use the properties of the Green function to accomplish such a task.

Two sub-classes of the BIM, known as the Boundary Element Method (BEM) and the Numerical Panel Method (NPM), have been used extensively to solve elliptic problems governed by the Poisson and Laplace equations. Even though the roots of all boundary integral methods are the same and it is hard to distinguish between the BEM and the NPM from a mathematical point of view, the implementation details of these two classes of boundary integral methods are different. Also, the NPM had been employed by engineers, mostly based on physical arguments, before any attempt was made to formalize the classical boundary element method.

The boundary element method is the subject of many well-written text books [3-5] and there are now a number of international journals devoted to the BEM algorithms and applications. The method has a rigorous and sound mathematical background and starts by providing a boundary integral formulation of the original differential equation. This integral equation is subsequently solved on a set of boundary elements. While applicable in both internal and external elliptic field problems, the BEM has been traditionally applied mostly in the solution of problems in closed domains. In particular, the BEM solution of conduction heat transfer problems in solids has been discussed in many text books [6-8] and journal papers [9,10]. Examples of the applications of the BEM in the solution of external flow problems can be found in [11,12].

The numerical panel method, on the other hand, has received a warm welcome from the external aerodynamic experts and has facilitated the development of a number of widely-used computational tools and computer codes for the solution of preliminary analysis and design problems in external aerodynamics. The NPM starts with the definition of the panels, which geometrically approximate the boundary shape, and then a number of singularity elements and collocation points are defined. The objective is to generate a harmonic field with prescribed boundary conditions by properly determining the strengths of the singularity elements. The mathematical simplicity and the ease of use, compared to the BEM, might explain the wider popularity of the NPM in the aviation industry. The rather lengthy papers by Hess and Smith [1] and Hess [13] and the textbook on low speed aerodynamics by Katz and Plotkin [14] are the classical references for students and engineers on the NPM. Other recent applications of the NPM include ship design [15,16] and the flow around propellers [17,18]. Here again, while the NPM is clearly applicable in both internal and external field problems, its application has been mostly limited to external ideal flow problems.

Therefore, in contrast to the continuing efforts on the numerical field approaches for the solution of elliptic problems [19,20], there are apparently no or very limited publications regarding the application of the NPM in bounded domains [21]. This paper, therefore, aims at filling the aforementioned gap and focuses on the application of the classical NPM in solving a class of elliptic problems in closed solution domains. More specifically, the paper provides the details of the implementation of the NPM in the context of the solution of the Laplace equation in bounded domains.

The paper includes the following sections. A brief description of the NPM in the context of external aerodynamics is provided in the next section followed by a discussion on the peculiarities associated with the application of the NPM in solving heat conduction problems in closed domains. Afterwards, a number of carefully selected test cases are presented. The examples cover a range of 2D problems in both singly- and doubly-connected domains which span over simple Cartesian to rather complex non-Cartesian geometries. The three commonly used standard boundary conditions, *i.e.* Dirichlet, Neumann and Robin boundary conditions, are also used in different combinations in the test cases. The NPM results in all cases are compared either to the available analytical solutions, where applicable, or the grid independent numerical

solutions obtained by the finite element method. The focus is then turned to the solution of flow problems in short ducts, *e.g.* the flow in the engine intake section of a propulsion system. The flow field in such cases can often be divided into a boundary layer and an inviscid ideal core flow. Examples of the application of the NPM in the solution of the core region of a number of internal flow problems wrap up this section of the paper. It should be noted that the inviscid core solution in an internal ideal flow has to be matched with the viscous (boundary layer) solution to approximate a real flow situation.

The NPM is clearly applicable in both two- and three-dimensional problems. However, to avoid the unnecessary time consuming logistics required in 3D solutions, the discussion here is limited to steady 2D problems. The grid refinement as well as the convergence acceleration has also been studied and carried out by the authors, but not reported here for the sake of briefness.

SOLUTION OF EXTERNAL AERODYNAMIC PROBLEMS VIA THE NPM

Figure 1a shows a non-lifting airfoil in a 2D free stream characterized by the far field uniform velocity $\vec{V}_\infty$. The airfoil disturbs the uniform flow in such a way that the velocity vector at a nearby point A, *i.e.* $\vec{V}_A$ shown in Figure 1a, is no longer equal to $\vec{V}_\infty$. The objective is to calculate the distribution of the scalar potential φ, which completely describes the ideal velocity field around the airfoil ($\vec{V} = \vec{\nabla}\varphi$). The constraints on the scalar potential are formally defined as follows:

$$\nabla^2\varphi = 0 \quad in \quad \Omega \tag{1a}$$

$$\vec{\nabla}\varphi \,.\hat{n} = 0 \quad on \quad \Gamma_b \tag{1b}$$

$$\vec{\nabla}\varphi = \vec{V}_\infty \quad for \quad (x,z) \to (\infty,\infty) \tag{1c}$$

The numerical panel method takes advantage of the linearity of the Laplace operator and employs the superposition of some singular solutions to model the effect of the geometry on the flow field and to approximately satisfy the boundary conditions on Γ_b. The flow patterns corresponding to a source and a doublet are shown in Figure 1b. A source (or sink) is described by its strength σ and results in a discontinuity, or jump, in the gradient of the scalar potential:

$$\sigma = \frac{\partial\varphi_E}{\partial n} - \frac{\partial\varphi_I}{\partial n} = V_E - V_I \tag{2}$$

Similarly, a doublet with the strength μ results in a potential jump as follows:

$$\mu = \varphi_E - \varphi_I \tag{3}$$

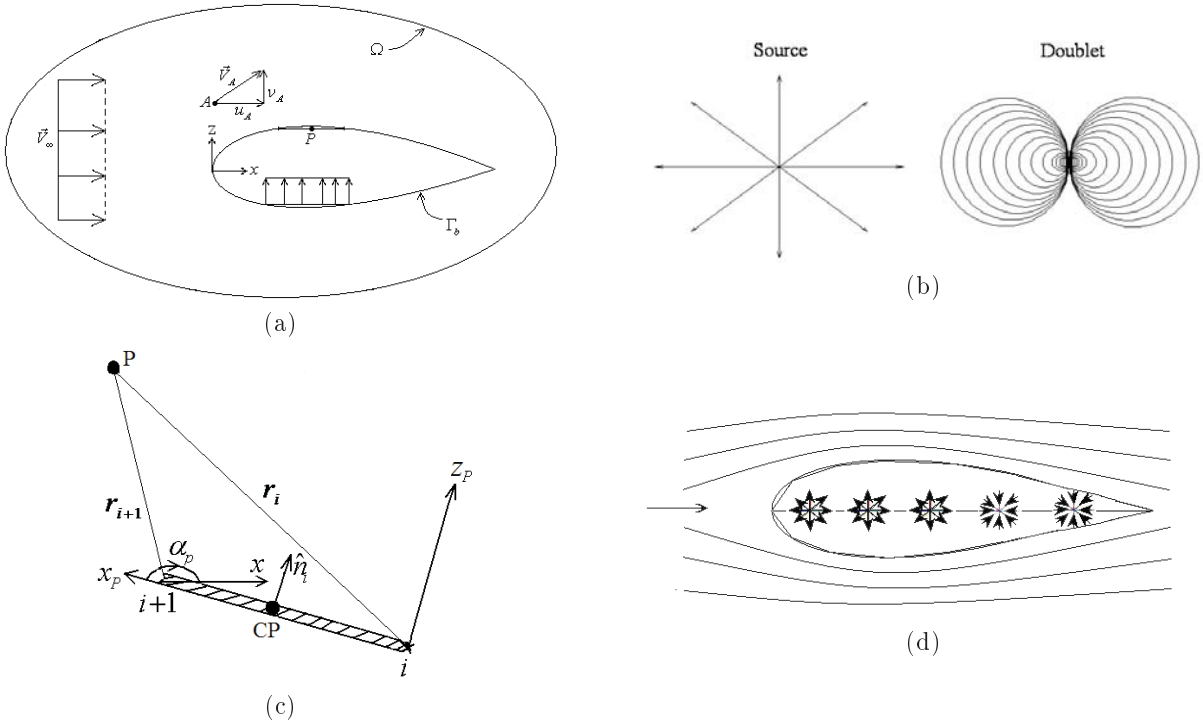

Figure 1. (a) Ideal flow around a non-lifting airfoil, the geometry and global coordinate system; (b) Source and doublet flow patterns; (c) A panel and its local coordinate system; (d) Finite number of sources and sinks along a chord line of the non-lifting airfoil.

An important feature of these elementary singularities is that they identically satisfy Eqs. (1a) and (1c). A typical collocation point C_P on the i^{th} boundary panel, *i.e.* the point of the implementation of Eq. (1b) on the panel, is shown in Figure 1c. Using a body-attached coordinate system and panels covered by source and doublet singularities, the Laplace equation and Green's third identity can be employed to develop the following integral constraint at an arbitrary collocation point [14]:

$$\varphi = \varphi_\infty + \frac{1}{2\pi}\int_{\Gamma_b} \sigma \ln r dl - \frac{1}{2\pi}\int_{\Gamma_b} \mu \frac{\partial(\ln r)}{\partial n} dl \qquad (4)$$

In Eq. (4), r is the distance between the panel and an arbitrary point P shown in Figure 1c.

If only source singularities are employed ($\mu = 0$), Eq. (4) can now be written as follows [14]:

$$\frac{\partial \varphi}{\partial n} = \frac{1}{2\pi}\int_{\Gamma_b} \sigma \frac{\partial(\ln r)}{\partial n} dl + \frac{\partial \varphi_\infty}{\partial n} \qquad (5)$$

Considering the fact that the normal velocity on the body is zero and $\partial\varphi_\infty/\partial n$ can be replaced by $\left(\vec{V}_\infty\right)$, and assuming uniform source panels, the constraint on the j^{th} source strength is obtained as follows:

$$\left(-\vec{V}_\infty\right)\cdot\vec{n}_j = \frac{1}{2\pi}\sum_{i=1}^{N}\left(\int_{\Gamma_{bi}} \sigma_i \frac{\vec{n}\cdot\vec{r}}{r^2} dl\right) \qquad (6)$$

The singularities are commonly distributed along the same panels which are used to discretize the boundary. However, it is also possible to employ separate singularity surfaces (panels). The singularity surfaces may be inside or outside of the solution domain. For example, it is intuitively clear that a finite number of sources

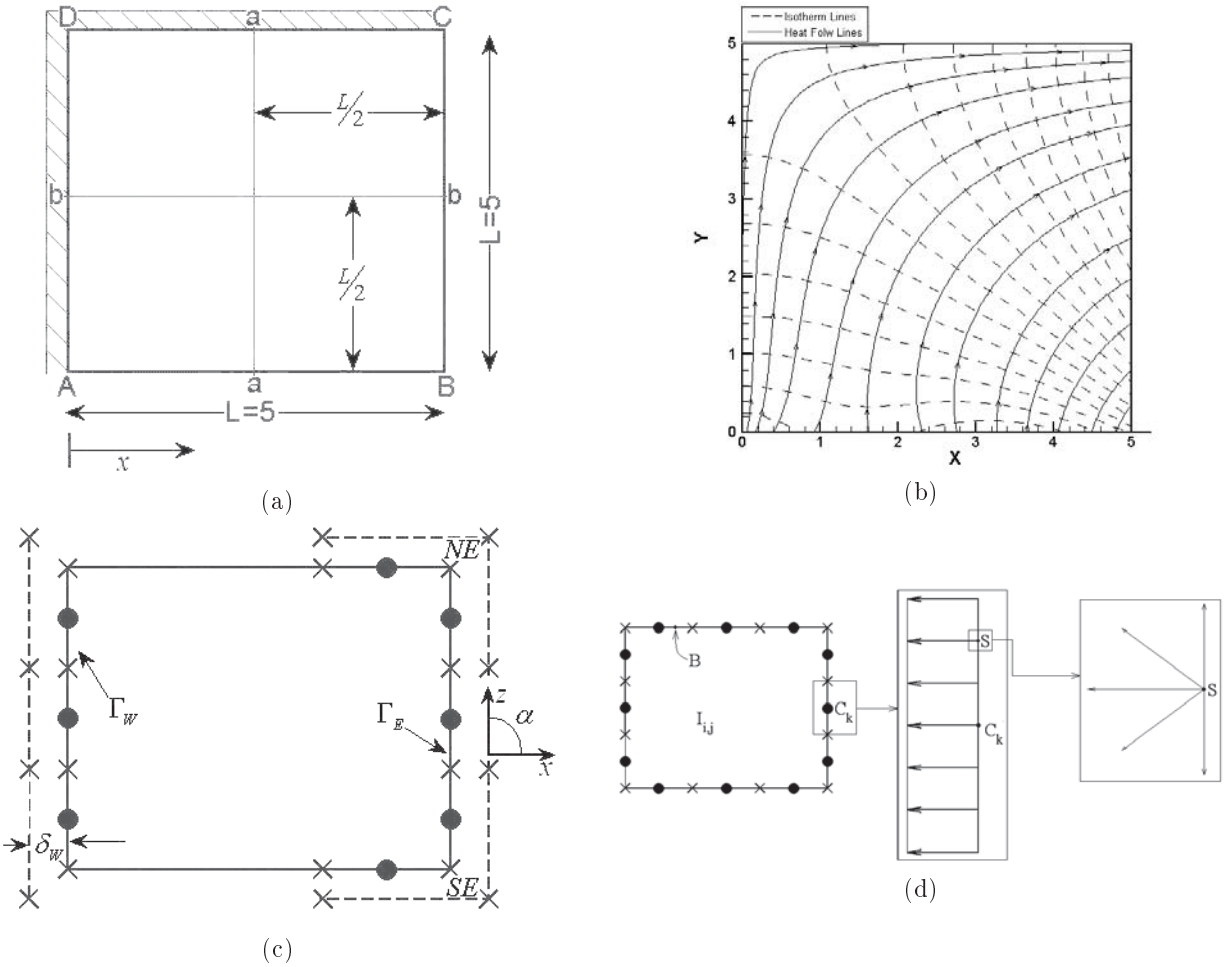

Figure 2. (a) The geometry of rectangular plate; (b) The isotherms and the heat flow lines in rectangular plate, analytical solution; (c) Panels and collocation points distributed around the plate; (d) Simple uniform source panels used in NPM solution.

and sinks along the chord line of the non-lifting airfoil shown in Figure 1d can be employed to push and pull the field lines in such a way that the body of the airfoil becomes a streamline. Here, it is seen that the panel surfaces containing the collocation points are not the same as the panel surfaces containing the singularities (*i.e.* singularity elements).

In practice, a variety of linear and nonlinear panel geometries can be used to model, in the discrete sense, the boundary, Γ_b. Other singularities, in addition to the sources and doublets, may also be employed [14]. Here, we restrict our discussion to the linear panel surfaces and uniformly distributed sources (sinks) and/or doublets.

The implementation of the NPM for the solution of the flow field around the airfoil shown in Figure 1a involves the following three steps:

1. Discretize the boundary Γ_b by a number of panels and define the collocation points along them.
2. Define the singularity elements.
3. Satisfy Eq. (1b) at all collocation points by properly determining the singularity strengths.

This requires the solution of a set of linear algebraic equations. In contrast to the numerical field methods, in which the sparse solvers are usually needed, the coefficient matrix corresponding to the algebraic set in the NPM is dense.

Once the set of algebraic equations is solved for the unknown singularity strengths (σ_i), the velocity at an arbitrary point in the flow field can be calculated using the following formula:

$$\vec{V}(x) = \vec{V}_\infty + \frac{1}{2\pi}\sum_{i=1}^{N}\left(\int_{\Gamma_{bi}} \sigma_i \frac{\vec{n}\cdot\vec{r}}{r^2} dl\right) \tag{7}$$

It is important to mention here that the Neumann boundary value problem described by Eq. (1) has an infinite number of solutions, because the level of the scalar potential field is not constrained. The multiplicity of the solution is particularly problematic in the calculation of the flow fields around lifting airfoils. The NPM includes the computational tasks necessary to single out the physically acceptable solution through the satisfaction of the Kutta condition. More information on the implementation of the Kutta condition can be found in aerodynamics text books [14].

SOLUTION OF STEADY HEAT CONDUCTION PROBLEMS VIA THE NPM

There is an analogy between the steady heat conduction problem and the external ideal flow problem. In addition to the similarity of the governing equations, the analogy also includes some physical parameters. For example, the normal heat flux component in heat conduction plays a role similar to the normal velocity component in potential flow. Also, the temperature corresponds to the scalar potential in such an analogy. However, in contrast to the aerodynamic problems, which are often solved around immersed boundaries and only need the implementation of the Dirichlet or Neumann boundary conditions, heat conduction problems are often solved in closed complex domains and the implementation of different types of boundary conditions on different parts of the boundary is often required.

To use the NPM in the context of heat conduction problems, three different kinds of singularity surfaces are employed here. These include uniform strength source panels, uniform strength doublet panels and uniform strength source-doublet panels and the methods which employ them are here referred to S-method, D-method and SD-method respectively. The details of the implementation of different boundary conditions on each of these cases are discussed in this section. Examples of the applications will be presented next.

The S-Method

The boundary-integral equation at a collocation point in this case, which is a simplified version of Eq. (4), is as follows:

$$T = \frac{1}{2\pi}\int_{\Gamma_b} \sigma(\ln r) dl \tag{8}$$

By taking the normal derivative, the following equation is also obtained:

$$\frac{\partial T}{\partial n} = \frac{1}{2\pi}\int_{\Gamma_b} \sigma \frac{\partial(\ln r)}{\partial n} dl \tag{9}$$

Now let's develop boundary integral equations for the three standard boundary conditions. To implement the Dirichlet boundary condition, $T = K$, Eq. (8) is used:

$$K = \frac{1}{2\pi}\int_{\Gamma_b} \sigma(\ln r) dl \tag{10}$$

To implement the Neumann boundary condition, $\partial T/\partial n = K'$, Eq. (9) is used as follows:

$$K' = \frac{1}{2\pi}\int_{\Gamma_b} \sigma \frac{\partial(\ln r)}{\partial n} dl \tag{11}$$

Finally, to implement the Robin boundary condition, $T + c(\partial T/\partial n) = K''$, both Eq. (8) and Eq. (9) are used as follows:

$$K'' = \frac{1}{2\pi}\left(\int_{\Gamma_b} \sigma(\ln r) dl + c\int_{\Gamma_b} \sigma \frac{\partial(\ln r)}{\partial n} dl\right) \tag{12}$$

To construct a numerical solution, the boundary is divided into N panels and the above equations are written as follows:

$$(K)_i = \sum_{j=1}^{N} \sigma_j B_{i,j} \tag{13}$$

$$(K')_i = \sum_{i=1}^{N} \sigma_i C_{i,j} \tag{14}$$

$$(K'')_i = \sum_{i=1}^{N} \sigma_j (C_{i,j} + cB_{i,j}) \tag{15}$$

In these equations, $B_{i,j}$ and $C_{i,j}$ are defined as $B_{i,j} = \frac{1}{2\pi}\int_{panel}(\ln r).dS$, $C_{i,j} = \frac{1}{2\pi}\int_{panel}\frac{\partial(\ln r)}{\partial n}dS$ and c is a constant parameter in the Robin boundary equation which is defined as a ratio between heat conduction coefficient, k_C, and heat convection coefficient, h_C, $c = k_C/h_C$.

Now, consider the rectangular plate shown in Figure 2a. All the space dimensions are normalized using a reference length. Whenever necessary, the metric units are used to assign dimensional numerical values. The heat conduction in this rectangular geometry can be mathematically described as follows:

$$\nabla^2 T = 0 \quad in \quad \Omega \tag{16a}$$

$$\vec{\nabla} T.\hat{n} = 0 \quad on \quad AD = \Gamma_{West} \tag{16b}$$

$$\vec{\nabla} T.\hat{n} = 0 \quad on \quad CD = \Gamma_{North} \tag{16c}$$

$$T = 50(\frac{x}{5})^2 + 20\sin(\frac{2\pi x}{5}) + 10 \quad on \quad AB = \Gamma_{South} \tag{16d}$$

$$T + c\frac{\partial T}{\partial x} = T_\infty \quad on \quad BC = \Gamma_{East} \quad (T_\infty = 500^\circ C) \tag{16e}$$

This boundary value problem can be analytically solved by the separation of variables method. The isotherms and the heat flow lines, obtained from the analytical solution, are shown in Figure 2b. Note that the temperature field T is a harmonic function and it is possible to generate the isotherms by a number of properly distributed harmonic field generators, *i.e.* singularities. Figure 2c shows the linear panels used to model the rectangular geometry. Each boundary panel is a 2D, uniform source line as shown in the close ups in Figure 2d. Assuming σ_i is the strength of the source line i per unit length, the objective is to determine the unknown singularities, *i.e.* σ_i, $i = 1, ..., N$, so that Eq. (16b) to Eq. (16e) are satisfied at the corresponding collocation points. Note that the field lines generated by each panel affect the thermal condition at the collocation points of all other panels. Therefore, satisfaction of the boundary condition at an arbitrary collocation point, P, whether it is Dirichlet (on, Γ_{South}), Neumann (on, Γ_{West} and, Γ_{North}) or Robin (on Γ_{East}), can be formulated in the following general form:

$$a_P \sigma_P + \sum_{nb=1,\neq P}^{N} a_{nb}\sigma_{nb} = (RHS)_P \tag{17}$$

In Eq. (17), a_P represents the influence of the singularity panel P on its corresponding collocation point, a_{nb} is the influence of the singularity panel nb on the collocation point P and the $(RHS)_P$ is any remaining constant term at the right hand side of the boundary condition equation at point P. Satisfaction of the boundary conditions at all collocation points is mathematically described by the following set of algebraic equations:

$$\begin{bmatrix} a_{11} & a_{12} & \dots & a_{1N} \\ a_{21} & a_{22} & \dots & a_{2N} \\ \vdots & \vdots & \ddots & \vdots \\ a_{N1} & a_{N2} & \dots & a_{NN} \end{bmatrix} \begin{Bmatrix} \sigma_1 \\ \sigma_2 \\ \vdots \\ \sigma_N \end{Bmatrix} = \begin{Bmatrix} (RHS)_1 \\ (RHS)_2 \\ \vdots \\ (RHS)_N \end{Bmatrix} \tag{18}$$

Once the unknown source strengths (σ_K, $K = 1, ..., N$) are known, it is possible to calculate the temperature T or the heat flux q at an arbitrary chosen internal or boundary point, *e.g.* $I_{i,j}$ or B in Figure 2d, using the following formulas:

$$T_I = \sum_{j=1}^{N} T_{I,j}\sigma_j \tag{19}$$

$$q_B = \sum_{j=1}^{N} q_{B,j}\sigma_j \tag{20}$$

In Eq. (19), $T_{I,j}$ represents the temperature influence of the singularity panel j on an arbitrary point, I, and $q_{B,j}$, in Eq. (20), is the flux influence of the singularity panel j on an arbitrary point B. Similar expressions can be obtained when the doublets or a combination of sources and doublets are used to generate the harmonic field.

The implementation of the NPM in the solution of a heat conduction problem is rather straight forward and involves the same computations as required in the solution of external aerodynamic problems. Since the temperature level is commonly constrained by the boundary conditions, the solution is unique and

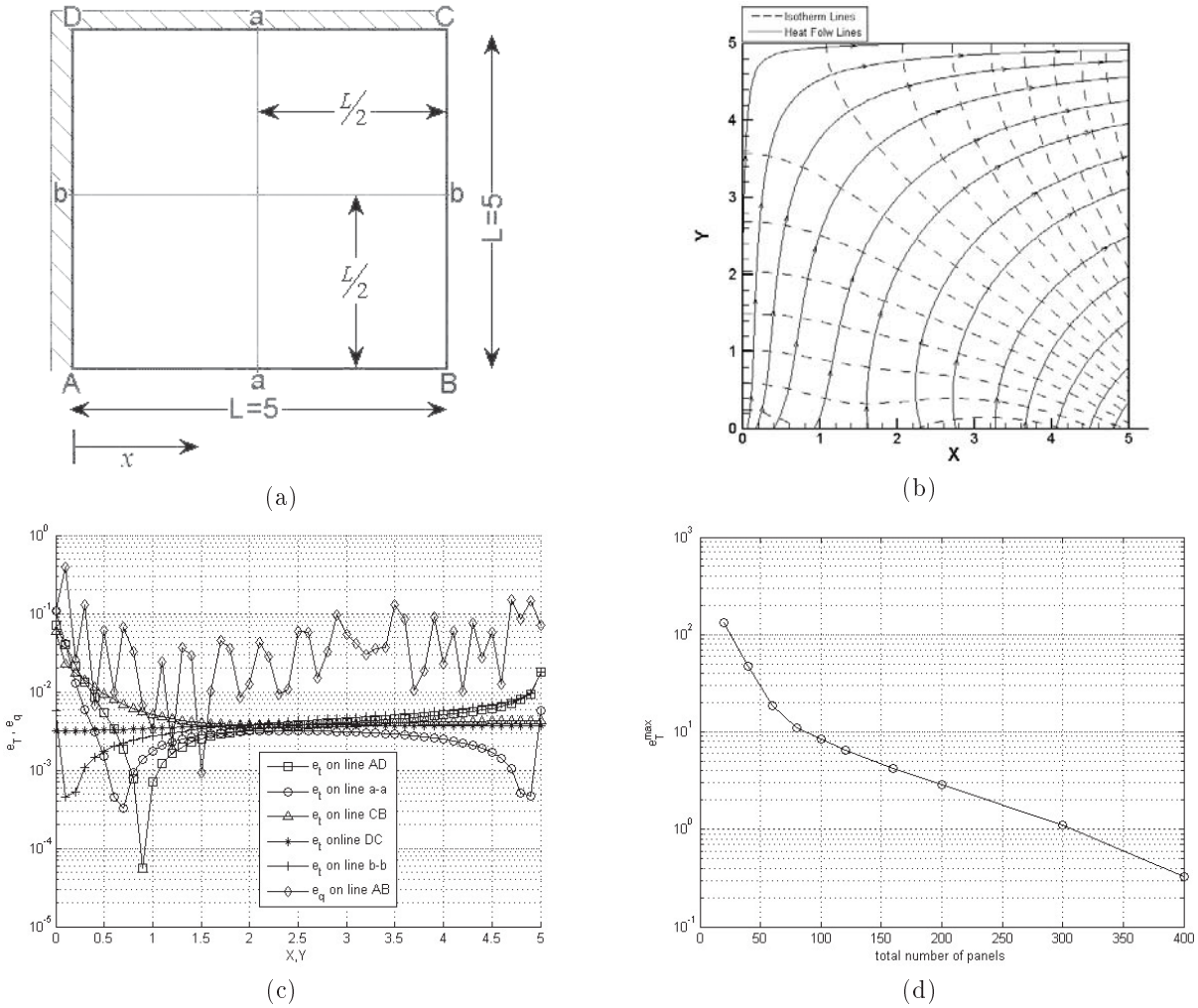

Figure 3. The S1 Test case: (a) The geometry; (b) The isotherms and the heat flow lines, calculated via the NPM; (c) The NPM error on lines a-a, A-D, C-B, D-C, b-b and A-B; (d) e^T_{max} versus number of panels.

there is no need for extra conditions similar to the Kutta condition. In a computer code for the implementation of the NPM, the information regarding the size and orientation of panels is needed. The required information is generated in a pre-processor which replaces the grid generation software in the classical numerical field solvers. Subroutines are also written to take care of the transformations between the local and global panel coordinates each time they are needed. The coordinates of the collocation points, the end points of the panels and the singularity lines are all the information that is required to carry out the computations in an NPM code.

The D-Method

Following the discussions in the previous section, the standard boundary conditions for the uniform strength doublet panels are implemented as follows:

The Dirichlet boundary condition:

$$(K)_i = \sum_{j=1}^{N} \mu_j C_{i,j} \tag{21}$$

The Neumann boundary condition:

$$(K')_i = \sum_{i=1}^{N} \mu_j D_{i,j} \tag{22}$$

The Robin boundary condition:

$$(K'')_j = \sum_{i=1}^{N} \mu_i (D_{i,j} + cC_{i,j}) \tag{23}$$

In these equations, $C_{i,j}$ is the same as the one defined in the previous section and, $D_{i,j} = \int_{panel} (\frac{\partial^2 \ln r}{\partial n^2})_i dl_i$.

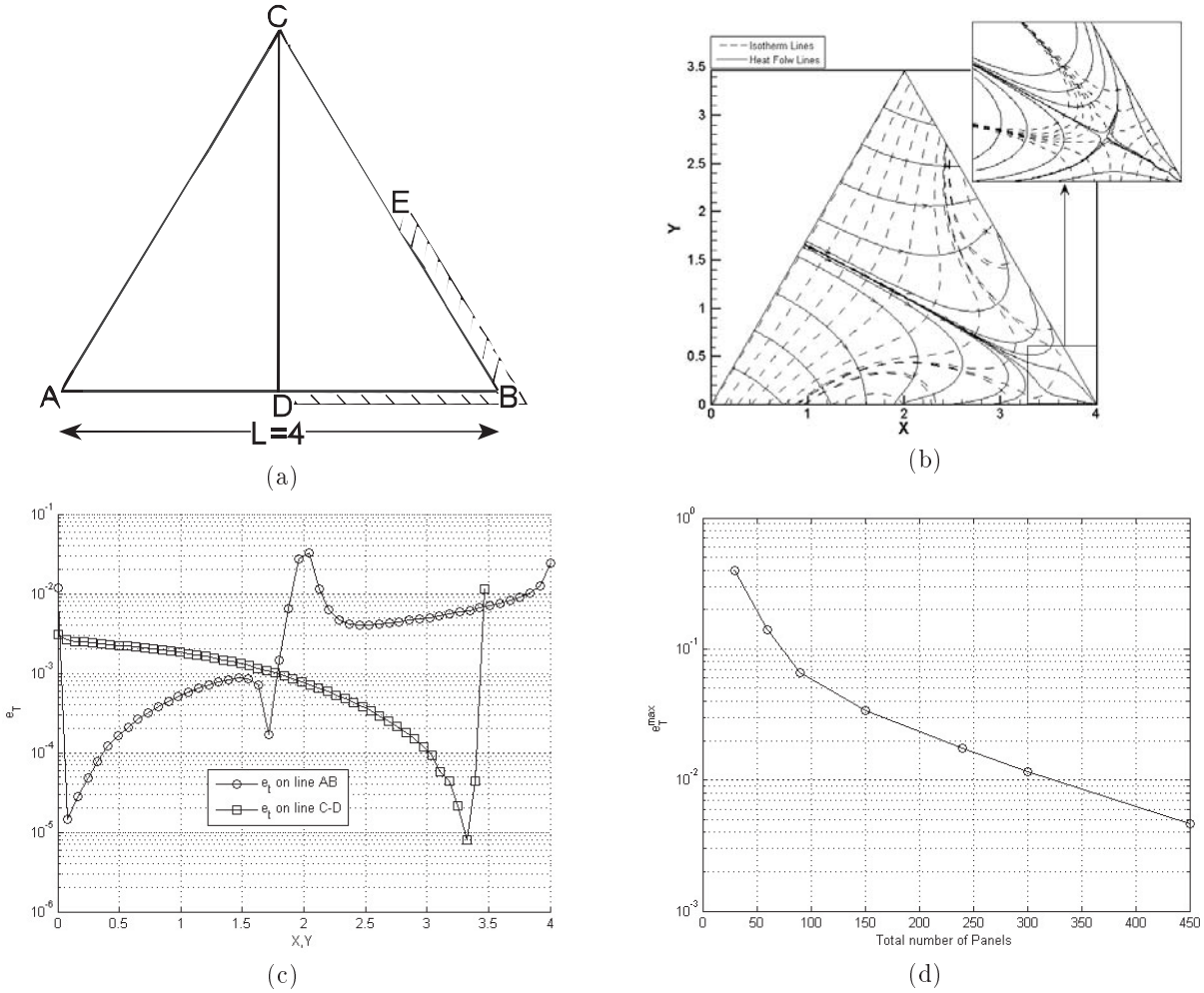

Figure 4. The S3 Test case: (a) the geometry; (b) The isotherms and the heat flow lines, calculated via the NPM; (c) The NPM error on lines A-B and C-D; (d) e^T_{max} versus number of panels.

The SD-Method

The discrete boundary-integral equation which can be obtained for the nodal temperature value in this case is as follows:

$$T = \sum_{j=1}^{N} B_{i,j}\sigma_j + \sum_{j=1}^{N} C_{i,j}\mu_j \tag{24}$$

Without losing the generality of the case, suppose that the temperature field is zero outside of the solution domain. In that case, Eq. (24) can be written in the following form for any external point:

$$\sum_{j=1}^{N} B_{i,j}\sigma_j + \sum_{j=1}^{N} C_{i,j}\mu_j = 0 \tag{25}$$

Typically, the collocation or control points are located at the middle of the panels. By slightly shifting the control points towards the exterior of the domain, Eq. (25) is applicable. Note that there are two unknown nodal values in Eq. (25). Therefore, either the source or the doublet strength needs to be user specified. To implement the Dirichlet boundary condition, $T = K$, recall that $\mu = T_E - T_I$. Since, $T_E = 0$, the doublet strength is constrained as follows:

$$\mu = -K \tag{26}$$

Therefore, Eq. (25) is written as follows:

$$\sum_{j=1}^{N} B_j(-\frac{\partial T_j}{\partial n}) = -\sum_{j=1}^{N} C_j(-K) \tag{27}$$

To implement the Neumann boundary condition, $\partial T/\partial n = K'$, recall that $\sigma = \partial T_E/\partial n - \partial T_I/\partial n$. Since $T_E = 0$ everywhere, we conclude that, $\partial T_E/\partial n = 0$. Hence, the source strength is constrained as follows in

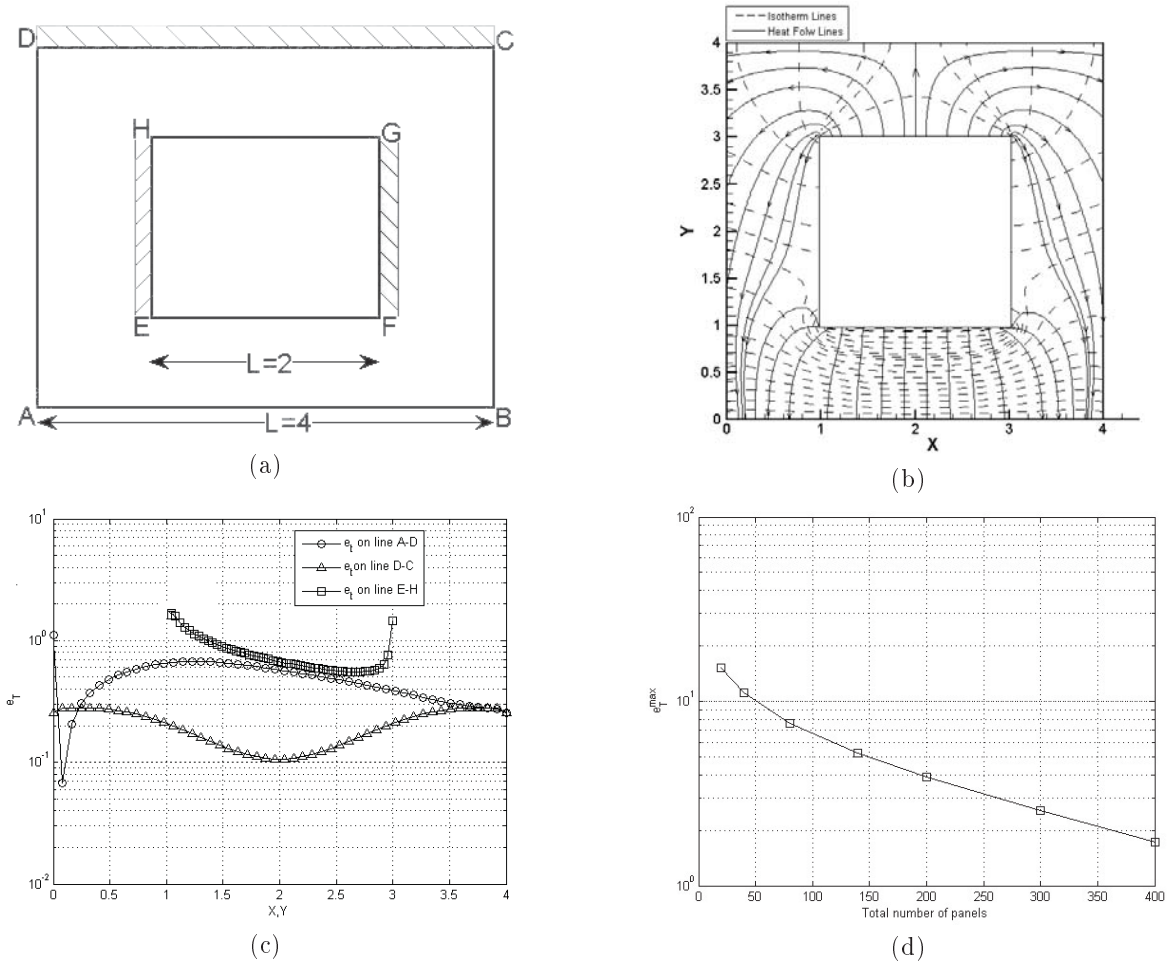

Figure 5. The S4 Test case: (a) the geometry; (b) The isotherms and the heat flow lines, calculated via the NPM; (c) The NPM error on lines A-D, D-C, E-H; (d) e^T_{max} versus number of panels.

this case:

$$\sigma = -\frac{\partial T_I}{\partial n} \tag{28}$$

Therefore, Eq. (25) changes to the following constraint in this case:

$$\sum_{j=1}^{N} C_j(-T_j) = -\sum_{j=1}^{N} B_j(-K') \tag{29}$$

A similar analysis shows that the implementation of the Robin boundary condition, $T + c(\partial T/\partial n) = K''$, results in the following boundary constraint:

$$\sum_{j=1}^{N} (cC_j + B_j)(\frac{\partial T_j}{\partial n}) = -\sum_{j=1}^{N} C_j(-K'') \tag{30}$$

Test Cases

Four problems are now investigated to show the applicability of the NPM in solving steady 2D heat conduction problems. All of these problems are solved by using uniform source elements. Problems 1 and 2 are also solved by uniform doublet elements and uniform source-doublet elements respectively. To evaluate the quality of the numerical solution, the NPM results are compared to either the analytical solution, wherever applicable, or the grid independent FEM solution which is referred to as the exact solution. Two error measures for the variable ϕ, which can be the temperature T or the heat flux q, are defined as follows:

$$e_\phi = (\left|\frac{\phi_i^{exact} - \phi_i^{panel}}{\phi_i^{exact}}\right|) \times 100 \quad i = 1, ..., N \tag{31}$$

$$e_\phi^{\max} = \max(\left|\frac{\phi_i^{exact} - \phi_i^{panel}}{\phi_i^{exact}}\right| \times 100) \quad i = 1, ..., N \tag{32}$$

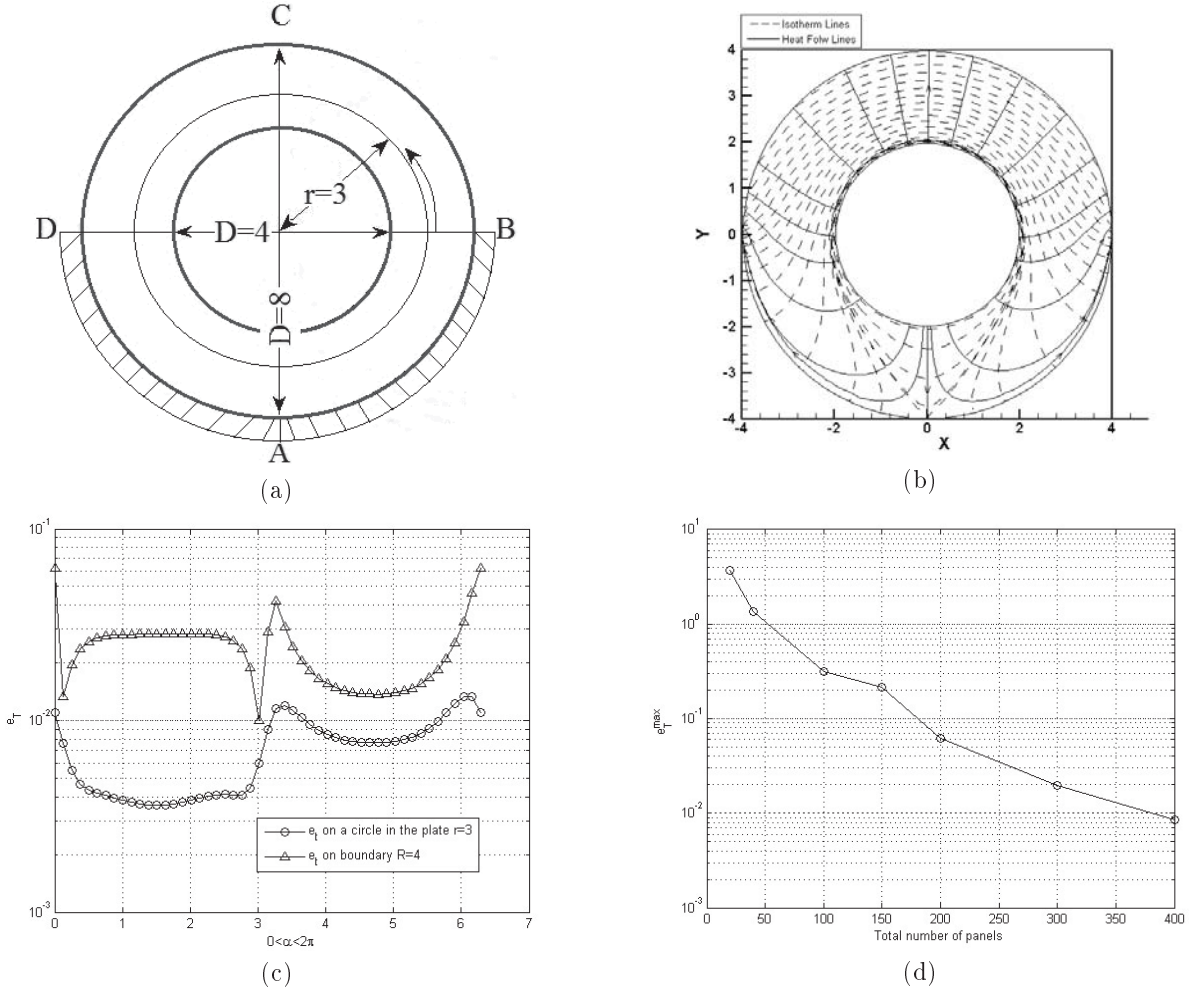

Figure 6. The S5 Test case: (a) The geometry; (b) The isotherms and the heat flow lines, calculated via the NPM; (c) The NPM error on the outer boundary of annular plate and on a circle, $r = 3$, in the annular plate; (d) e^T_{max} versus number of panels.

The S1 Test Case

Figure 3a shows a simply connected rectangular domain with the following boundary conditions:

$$\begin{cases} \vec{\nabla}T.\hat{n} = 0 \quad on \quad AD\&CD \\ T = 50(\frac{x}{L})^2 + 20\sin(\frac{2\pi x}{L}) + 10 \quad on \quad AB \quad (L = 5m) \\ T + c\frac{\partial T}{\partial x} = T_\infty \quad on \quad BC \quad T_\infty = 500°C \end{cases}$$

The isotherms and the heat flow lines, calculated via the NPM, are shown in Figure 3b. A 50×50 uniform Cartesian grid is used to generate the internal points for the calculation of the nodal values of the scalar temperature and the heat flux vector. This corresponds to 49 panels at each side of the rectangular plate. The solution error at the boundaries and at the internal nodes located on lines a-a, and b-b in Figure 3a are shown in Figure 3c. For the internal nodes, the calculated temperatures are compared to the analytical solution to report the temperature error (e_T). However, at the boundary AB, the calculated heat flux is compared to the analytical value to determine the heat flux error (e_q). Note that the maximum error occurs on the boundary AB near the corner point A and all of the calculated errors are less than 0.1%. Dependency of ($e_T^{\max}$) upon the number of panels is shown in Figure 3d.

The S2 Test Case

Figure 4a shows a simply connected triangular domain with the following boundary conditions:

$$\begin{cases} \vec{\nabla}T.\hat{n} = 0 \quad on \quad BD\&EB \\ T + c\frac{\partial T}{\partial x} = T_\infty \quad on \quad CE\&AD \quad (T_\infty = 20°C) \\ T = 100°C \quad on \quad AC \end{cases}$$

The isotherms and the heat flow lines, calculated via the NPM, are shown in Figure 4b. These results correspond to a uniform computational grid with 2500

internal nodes. The solution error at the boundaries and at the internal nodes, located along the line CD in Figure 4a, are shown in Figure 4c. The solution corresponds to 100 panels at each side of the triangular plate. For the internal nodes, the calculated temperatures are compared to the grid independent FEM solution to report the temperature error (e_T). Note that the maximum error occurs near the corner points or near the points where a boundary condition switches to another one. Dependency of ($e_T^{\max}$) upon the total number of panels is shown in Figure 4d.

The S3 Test Case

Figure 5a shows a multiply connected rectangular domain with the following boundary conditions:

$$\begin{cases} \vec{\nabla}T.\hat{n} = 0 \quad on \quad CD, EH\&FG \\ T + c\frac{\partial T}{\partial x} = T_\infty \quad on \quad AD\&BC \quad (T_\infty = 30°C) \\ T = 10°C \quad on \quad AB \\ T = 50°C \quad on \quad EF\&GH \end{cases}$$

The isotherms and the heat flow lines, calculated via the NPM, are shown in Figure 5b. The solution error at the external boundaries and at the internal boundary nodes along the line EH in Figure 5a are shown in Figure 5c. This solution corresponds to 50 panels at each side of the outer boundary and 50 panels at each side of the inner boundary. For the internal boundary nodes, the calculated temperatures are compared to the grid independent FEM solution to report the temperature error (e_T). Note that the maximum error occurs on the internal boundary near the corner points H and E. Note that these are also the switch over points of the boundary conditions. Dependency of ($e_T^{\max}$) upon the number of panels is shown in Figure 5d.

The S4 Test Case

Figure 6a shows a multiply connected circular domain with the following boundary conditions:

$$\begin{cases} \vec{\nabla}T.\hat{n} = 0 \quad on \quad CA\&AD \\ T = 100°C \quad on \quad Internal\ Circle \\ \frac{h_C}{k_C} \times (T - T_\infty) + \left(\frac{\partial T}{\partial x}\right) = 0 \\ \qquad on \quad CB\&BD \ (T_\infty = 20°C) \end{cases}$$

The isotherms and the heat flow lines, calculated via the NPM, are shown in Figure 6b. The solution error at the boundaries and at the internal nodes located along the internal circle ($r = 3$) in Figure 6a are shown in Figure 6c. The presented numerical solution corresponds to 200 panels on the outer boundary and 200 panels on the inner boundary. For the internal nodes, the calculated temperatures are compared to the grid independent FEM solution to report the temperature error (e_T). It is seen that the NPM solution is more accurate at internal nodes. Dependency of the error upon the number of panels is shown in Figure 6d.

The D1 Test Case

The test case S1 is now solved via the uniform doublet lines. The solution error on the boundary and at the internal nodes located along the line a-a and b-b in Figure 3a are shown in Figure 7a. Dependency of ($e_T^{\max}$) upon the total number of panels in this case is shown in Figure 7b. It can be seen that the error (e_T) in this case is less than the error of the solution obtained via the source panels. However, the heat flux error (e_q) in this case is more than the error obtained via the source panels.

Another observation is that the order of accuracy, *i.e.* the rate of decrease in ($e_T^{\max}$) with the total number of panels, is less when doublet panels are employed.

The SD1 Test Case

Finally, the test case S3 is solved via uniform source-doublet lines. The solution errors on the boundaries and at the internal nodes along the line CD in Figure 4a are shown in Figure 7c. Dependency of ($e_T^{\max}$) upon the total number of panels is shown in Figure 7d. Again, it is observed that the order of accuracy is increased as compared to the source panel case.

PANEL METHOD IN INTERNAL IDEAL FLOWS

To implement the panel method in an internal flow, one should take into the consideration the following points:

1. In contrast to the external flow problems, in which either the Dirichlet or the Neumann boundary condition is imposed on the body, different types of boundary conditions may be imposed simultaneously in an internal flow problem.
2. There is no far-field boundary in internal flow problems and the whole domain is surrounded by singularities.
3. To obtain accurate results, the corner points need special treatments.

Implementation of the Panel Method in Internal Flows

Consider the simple diffuser shown in Figure 8. As mentioned before all space dimensions are normalized using a reference length. Whenever necessary, the metric units are used to assign dimensional numerical values.

Neumann boundary conditions are imposed at the inlet and side boundaries and the Dirichlet boundary condition is imposed at the outlet. To construct a numerical solution, the boundary is divided into N panels. By satisfying the boundary conditions at points a and b in Figure 8, one obtains:

$$\sum_{j=1}^{N} C_{a,j}\sigma_j = U_{in} \tag{33}$$

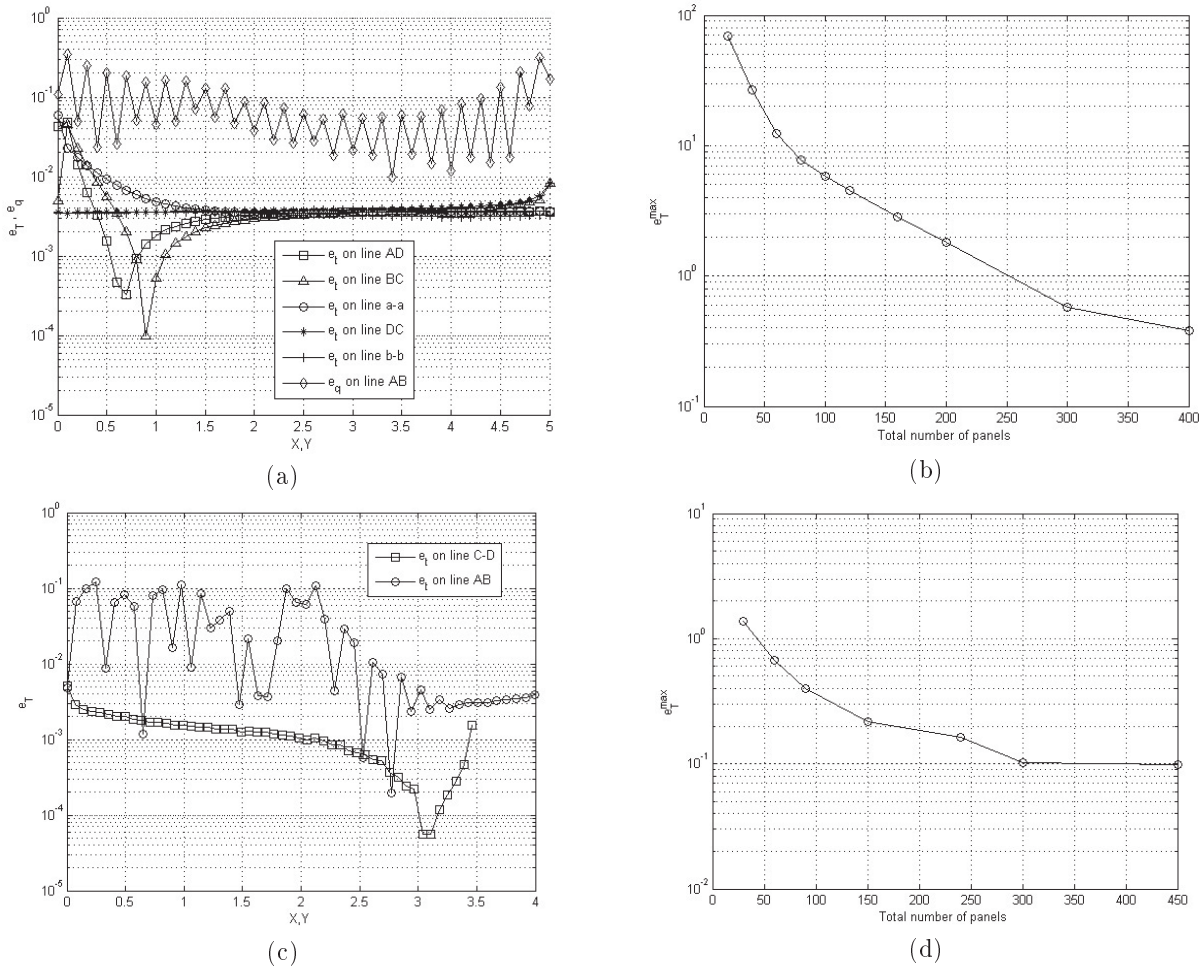

Figure 7. The D1 and the D2 Test case: (a) The NPM error on lines a-a, A-D, C-B, D-C, b-b and A-B (Figure 3a); (b) e^T_{max} versus number of panels in a rectangular plate; (c) The NPM error on lines A-B and C-D (Figure 4a); (d) e^T_{max} versus number of panels in a rectangular plate.

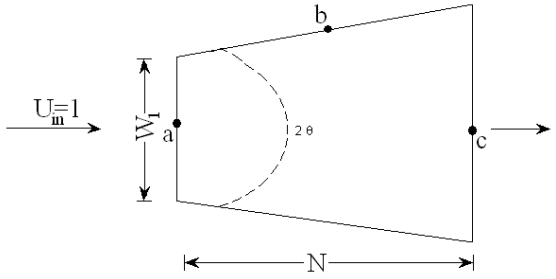

Figure 8. CA simple, two-dimensional diffuser.

$$\sum_{j=1}^{N} B_{b,j}\sigma_j = 0 \tag{34}$$

For the non-penetrative walls of the diffuser, the Neumann boundary condition is imposed:

$$\sum_{j=1}^{N} C_{c,j}\sigma_j = 0 \tag{35}$$

In these equations, $B_{i,j}$ and $C_{i,j}$ are defined as $B_{i,j} = \frac{1}{2\pi}\int_{panel}(\ln r).dS, C_{i,j} = \frac{1}{2\pi}\int_{panel}\frac{\partial(\ln r)}{\partial n}dS$ in which i indicates the collocation point.

The Dirichlet and Neumann boundary conditions can be recast in the following general form:

$$a_P\sigma_P + \sum a_{nb}\sigma_{nb} = (RHS)_P \tag{36}$$

In Eq. (36), a_P represents the influence of the singularity panel P on its corresponding collocation point, a_{nb} is the influence of the neighboring singularity panels on the collocation point P and the $(RHS)_P$ is any remaining constant term at the right hand side. Satisfaction of the boundary conditions at all

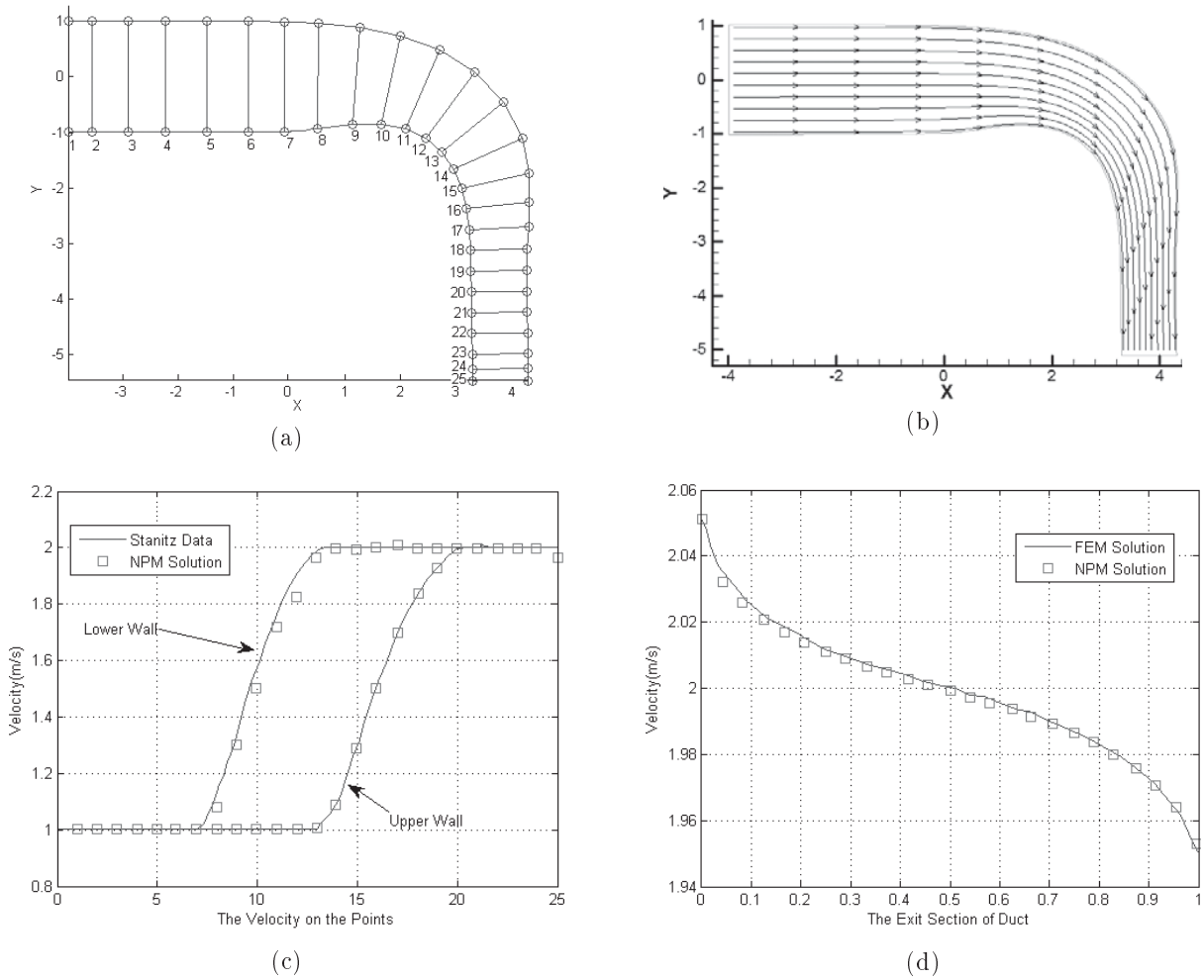

Figure 9. The SI1 Test case: (a) The geometry; (b) The streamline, calculated via the NPM; (c) The velocities at the boundaries (AD, BC); (d) The velocities at the outlet section (CD).

collocation points is mathematically described by the following set of algebraic equations:

$$\begin{bmatrix} a_{11} & a_{12} & \dots & a_{1N} \\ a_{21} & a_{22} & \dots & a_{2N} \\ \vdots & \vdots & \ddots & \vdots \\ a_{N1} & a_{N2} & \dots & a_{NN} \end{bmatrix} \left\{ \begin{array}{c} \sigma_1 \\ \sigma_2 \\ \vdots \\ \sigma_N \end{array} \right\} = \left\{ \begin{array}{c} (RHS)_1 \\ (RHS)_2 \\ \vdots \\ (RHS)_N \end{array} \right\} \tag{37}$$

Once the unknown source strengths (σ_K, $K = 1, ..., N$) are obtained, it is possible to calculate the velocity V_I at an arbitrary point, I, by the following formula:

$$V_I = \sum_{j=1}^{N} u_{I,j}\sigma_j \tag{38}$$

$u_{I,j}$, in Eq. (38), is the velocity influence of the singularity panel j on an arbitrary point, I.

Test cases

Three test cases are now discussed to show the applicability of the NPM in the solution of internal flow problems. All of these problems are solved by using uniform source lines. To evaluate the quality of the numerical solution, the NPM results are compared to the grid independent FEM solution which is referred to as the exact solution.

The SI1 Test Case

Figure 9a shows a nozzle with the following boundary conditions:

$$\left\{ \begin{array}{l} \vec{V}.\hat{n} = 0 \quad on \quad BC\&AD \\ \vec{V}.\hat{n} = U_{in} \quad on \quad AB \quad (U_{in} = 1\, m/s) \\ \varphi = 0 \quad on \quad CD \quad (\vec{V} = \frac{\partial \varphi}{\partial n}) \end{array} \right.$$

The streamlines, calculated via the NPM, are shown in Figure 9b. These results correspond to a uniform

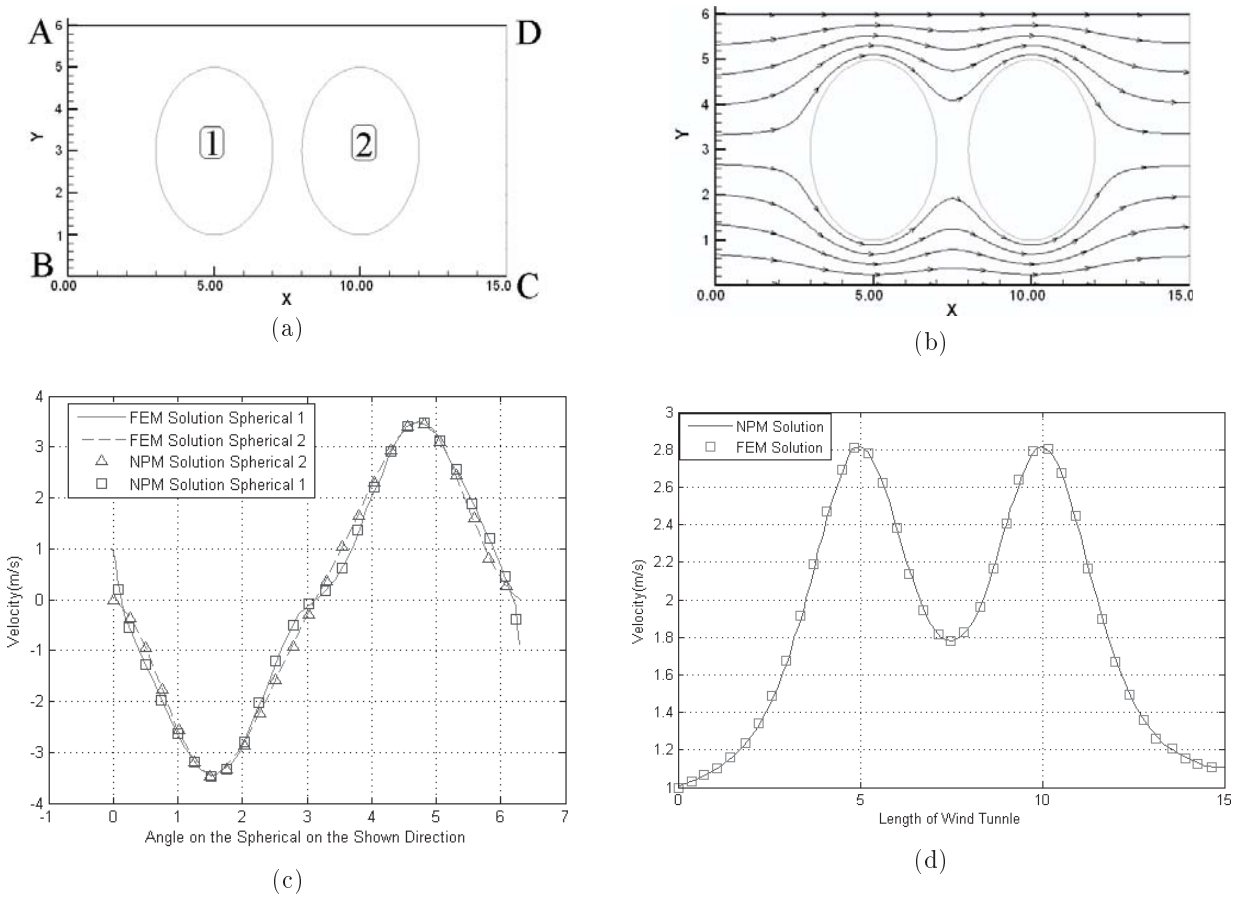

Figure 10. The SI2 Test case: (a) The geometry; (b) The streamline, calculated via the NPM; (c) The velocities on the cylinders (1,2) ;(d) The velocities at the boundary (BC).

computational grid with 2500 internal nodes. This solution corresponds to 400 panels at the boundary of the nozzle. Velocities at the boundaries, (BC and AD), are compared to the grid independent FEM solution and are shown in Figure 9c. Velocities at the outlet section of the nozzle are also compared to the grid independent FEM solution and are reported in Figure 9d. Good agreements are observed in both cases.

The SI2 Test Case

Figure 10a shows two cylinders in a short duct with the following boundary conditions:

$$\begin{cases} \vec{V}.\hat{n} = 0 \quad on \quad BC, AD \,\&\, on\, the\, cylinders \\ \vec{V}.\hat{n} = U_{in} \quad on \quad AB \quad (U_{in} = 1\, m/s) \\ \varphi = 0 \quad on \quad CD \end{cases}$$

The streamlines, calculated via the NPM, are shown in Figure 10b. These results correspond to a uniform computational grid with 2500 internal nodes, 400 panels at the boundaries and 100 panels on the cylinders. Velocities at the boundary, (AD), are compared to the grid independent FEM solution and are shown in Figure 10c. Velocities on the cylinders are also compared to the grid independent FEM solution and are reported in Figure 10d. Good agreements are observed in both cases.

The SI3 Test Case

Figure 11a shows an airfoil (NACA0012) in a short duct with the following boundary conditions:

$$\begin{cases} \vec{V}.\hat{n} = 0 \quad on \quad BC, AD \,\&\, on\, the\, airfoil \\ \vec{V}.\hat{n} = U_{in} \quad on \quad AB \quad (U_{in} = 1\, m/s) \\ \varphi = 0 \quad on \quad CD \end{cases}$$

The streamlines, calculated via the NPM, are shown in Figure 11b. These results correspond to a uniform computational grid with 2500 internal nodes, 400 panels at the outer boundaries and 100 panels on the airfoil. Pressure coefficients, $C_p = 1 - U^2/U_\infty^2$, on the airfoil are compared to the grid independent FEM solution and to the solution for a free stream situation. Results have been reported for two different widths ($D = 0.7$ and $D = 2$) and are shown in Figure 11c and Figure 11d. As shown in the figures, the results

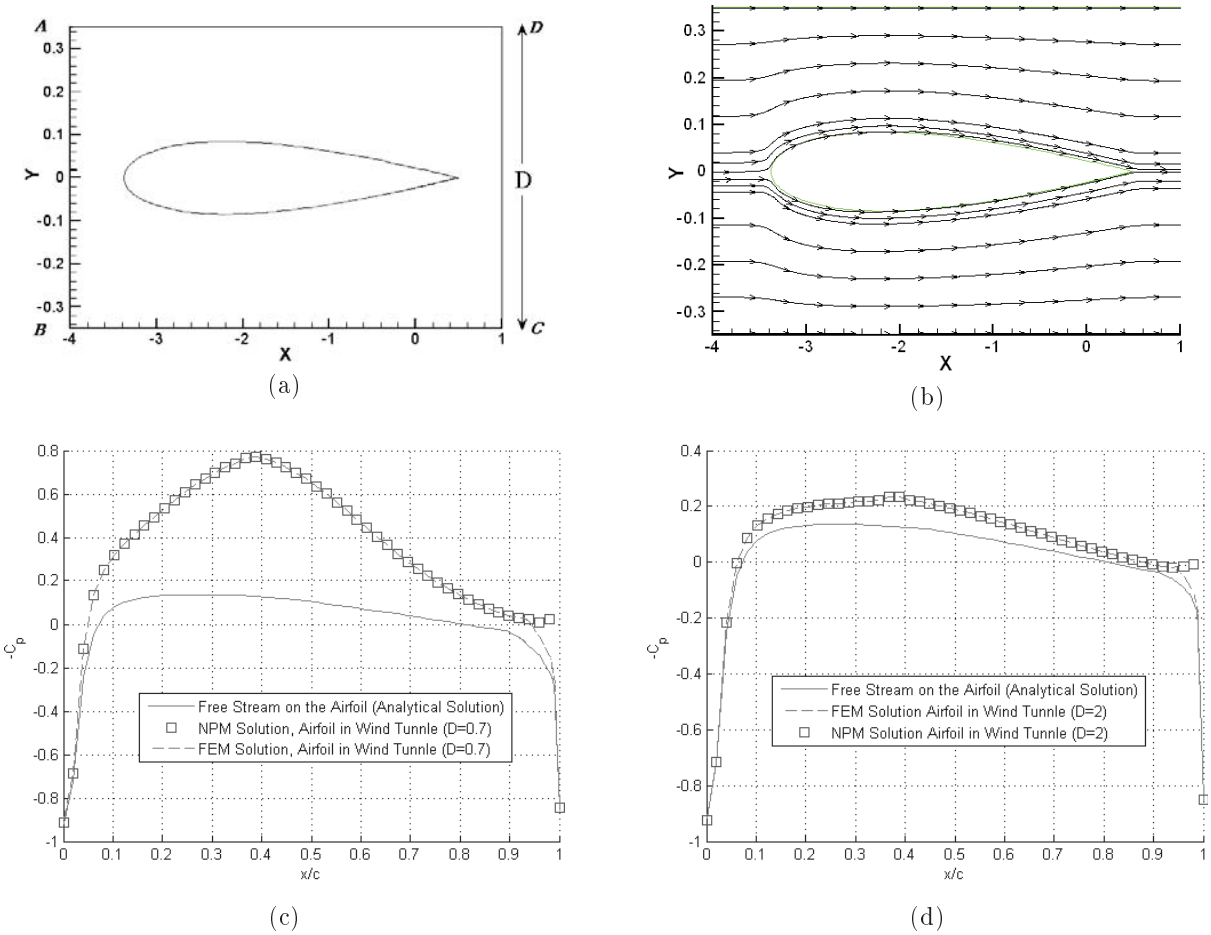

Figure 11. The SI3 Test case: (a) The geometry; (b) The streamline, calculated via the NPM; (c) Pressure coefficients on the airfoil (D=0.7) ;(d) Pressure coefficients on the airfoil (D=2).

are closer to the free stream solution for the short duct with the larger width as expected.

CONCLUSION

The classical numerical panel method was employed to solve a number of steady two-dimensional heat conduction and internal ideal flow problems. Three panel methods, *i.e.* the S-Method, the D-Method and the SD-Method, were introduced and employed to solve various problems with fairly complex geometries and boundary conditions. Both analytical solutions and accurate finite element results were used for the validation. Only the S-Method was used to solve all of the test problems and the results of the other methods were compared to the S-Method for just a number of cases. The results show that the panel methods can be reliably used to solve complex heat conduction as well as internal ideal flow problems. Both the accuracy and the speed of the computations can be improved by using refined grids and convergence acceleration techniques not discussed here.

REFERENCES

1. Hess J.L., Smith A.M.O., "Calculation of Potential Flow about Arbitrary Bodies", *Journal of Heat Transfer*, **1**, PP 1-138(1967).

2. Parhizkar H., Karimian M.H., Mani M., "Numerical Simulation of Flow Past Oscillating Airfoil Using Oscillation of Flow Boundary Condition", *Journal of Aerospace Science and Technology (JAST)*, **3**(1), PP 17-22(2006).

3. Banerjee P.K., *The Boundary Element Method in Engineering*, McGraw Hill Book Co., .

4. Ramachandran P.A., "Boundary Element Methods in Transport Phenomena", *Comp. Mech. Publication. Elsevier Applied Science*, (1994).

5. Brebbia C.A., "Boundary Element Techniques in Computer-Aided Engineering", *Springer Publication*, (2007).

6. Taler J., Duda P., "Solving Direct and Inverse Heat Conduction Problems", *Springer Publication*, (2007).

7. Necati M., "Boundary Value Problems of Heat Conduction", *Dover Publication*, (2002).

8. Divo E.A., Kassab A.J., "Boundary Element Method for Heat Conduction with Application in Non-Homogeneous Media", *Mc GRAW HILL*, (2003).
9. Divo E.A., Kassab A.J., "A Boundary Integral Equation for Steady Heat Conduction in Anisotropic and Heterogeneous Media", *Numerical Heat Transfer*, **32**(1), PP 37-61(1997).
10. WeiGao X., Wang J., "Interface Integral BEM for Solving Multi-medium Heat Conduction Problems", *Engineering Analysis with Boundary Elements*, **33**(4), PP 539-546(2009).
11. Carey G.F., Kim S.W., "Lifting Aerofoil Calculation Using the Boundary Element Methods", *International Journal for Numerical Methods in Fluids*, **3**, PP 481-492(1983).
12. Rashidi I., Moin H., Fard Mo. P., Fard Ma. P., "Numerical Simulation of Partial Cavitation Over Axisymmetric Bodies VOF Method vs. Potential Flow Theory", *Journal of Aerospace Science and Technology (JAST)*, **5**(1), PP 23-34(2008).
13. Hess J.L., "Panel Method in Computational Fluid Dynamics", *Annu. Rev. Fluid Mech.*, (1990).
14. Plotkin A., Katz J., *Low-Speed Aerodynamics*, Cambridge University Press, (2001).
15. Tarafder M.D.S., Suzuki K., "Numerical Calculation of Free-Surface Potential Flow Around a Ship Using a Modified Rankine Source Panel Method", *Ocean Engineering*, **35**, PP 536-544(2008).
16. Yoo J., "Design of Ship's Bow Form by Potential Base Panel Method", *Ocean Engineering*, **34**(8-9), PP 1089-1095(2007).
17. Wing Y.J., Ying X., "Prediction of Podded Propeller Cavitation Using an Unsteady Surface Panel Method", *Journal of Hydrodynamics*, **20**(6), PP 790-796(2008).
18. Wong L.B., Zhang L., Zang N.D., "A Potential Flow 2D Vortex Panel Method: Applications to Vertical Axis Straight Blade Tidal Turbine", *Energy Convection and Management*, **48**, PP 457-461(2007).
19. Frouzan-sepehr S., Mohammadi S., "A Fast Mesh-Free Galerkin Method for the Analysis of Steady-State Heat Transfer", *Journal of Aerospace Science and Technology (JAST)*, **6**(1), PP 13-23(2009).
20. Liu Y., Zhang X., Lu M., "Meshless Least-Squares Method for Solving the Steady-State Heat Conduction Equations", *Tsinghua Science & Technology*, **10**(1), PP 61-66(2005).
21. Ashby D.L., Sandline D.R., "Application of Low Order Panel Method to Complex Three-Dimensional Internal Flow Problems", *NASA Contractor Report 177424* , (1986).